Received: 23 August 2017 | Revised: 17 January 2018 | Accepted: 19 January 2018
DOI: 10.1002/rcs.1901

WILEY The International Journal of Medical Robotics and Computer Assisted Surgery

ORIGINAL ARTICLE

Development of a new 3-DOF parallel manipulator for minimally invasive surgery

Alaa Khalifa[1] | Mohamed Fanni[1,2] | Abdelfatah M. Mohamed[1,3] | Tomoyuki Miyashita[4]

[1]Department of Mechatronics and Robotics Engineering, Egypt–Japan University of Science and Technology, E-JUST, New Borg El-Arab City, Alexandria, Egypt
[2]On leave from Department of Production Engineering and Mechanical Design, Mansoura University, Mansoura, Egypt
[3]On leave from Department of Electrical Engineering, Assiut University, Egypt
[4]Department of Modern Mechanical Engineering, Faculty of Science and Engineering, Waseda University, Japan

Correspondence
Alaa Khalifa, Department of Mechatronics and Robotics Engineering, Egypt–Japan University of Science and Technology, E-JUST, New Borg El-Arab City, Alexandria, Egypt.
Email: alaa.khalifa@ejust.edu.eg

Abstract

This article proposes a novel dexterous endoscopic parallel manipulator for minimally invasive surgery. The proposed manipulator has 3 degrees of freedom (3-DOF), which consist of two rotational DOFs and one translational DOF (2R1T DOFs). The manipulator consists of 3 limbs exhibiting identical kinematic structure. Each limb contains an active prismatic joint followed by 2 consecutive passive universal joints. The proposed manipulator has a unique arrangement of its joints' axes. This unique arrangement permits large bending angles, ±90° in any direction, and a workspace almost free from interior singularities. These advantages allow the proposed manipulator to outperforms existing surgical manipulators. However, this unique arrangement makes the analysis of the robot extremely difficult. Therefore, a geometrical/analytical approach is used to facilitate its singularity analysis. Construction of the virtual prototype is accomplished using ADAMS software to validate the proposed manipulator and its bending capability. A closed-form solution for inverse kinematics is obtained analytically. Also, the forward kinematics solution is obtained numerically. Moreover, evaluation of the workspace is achieved using motion/force transmissibility indices. A practical experiment has been performed using a scaling technique and PID controller. The experimental results show the feasibility of the teleoperated surgical system using the proposed parallel manipulator as the slave.

KEYWORDS
architecture singularity, constraint singularity, minimally invasive surgery, parallel manipulator, reciprocal screw, surgical robots

1 | INTRODUCTION

Generally, clinical endoscopic manipulators are divided into two categories: serial and parallel manipulators. Serial manipulators are utilized as parts in current commercial surgical systems. These manipulators depend on wires to transmit the mechanical movement to the robot joints since no actuators are allowed inside the patient's body. There are two well-known commercial systems that utilize serial manipulators. The first one is the da Vinci system delivered by Intuitive Surgical, Inc.[1] Furthermore, this is the one that is currently used in hospitals. The second one is the Zeus system delivered by Computer Motion, Inc.,[2] which is no longer used in hospitals nowadays. Although the utilization of wire-driven surgical manipulators has spread widely, it has many disadvantages, for example, troubles during the sterilization process in endoscopic applications. Likewise, the wire might rupture during the operation, and the surgeon would be compelled to finish the operation by hand. Besides, in tendon-driven manipulators, the wire can pull but cannot push, which complicates the system. Additionally, the wires might be slack and a pre-tensioning mechanism be required. In order to avoid these issues, researchers have started to propose parallel manipulators where the active joints are located at the base, which makes their actuation using flexible shafts (flexible tubes) easier than that of serial manipulators.

The second category of surgical manipulators is parallel ones. A parallel manipulator (PM) is characterized as a closed-loop mechanism in which its movable platform is connected with the fixed-base platform through several independent kinematic chains. Specifically, parallel manipulators have huge potential applications because of their potential preferences compared with those of serial manipulators. These preferences are large payload capacity, high structural stiffness,

accurate positioning and high speed. In addition, their applications in the therapeutic field are characterized by the easiness of the sterilization procedure and the avoidance of the use of wires.

A robotic forceps[3] has been developed that can bend in 2 dimensions but the bending angles cannot exceed ±70°. A new dual-screw-drive (DSD) forceps has been developed by Ishii *et al.*[4] However, the manufacturing accuracy needs to be improved. An endoscopic forceps manipulator was introduced by Yamashita *et al.*[5] It has 2-DOFs to bend the manipulator using multiple slider linkage mechanisms. Several problems with the precision and power consumption have been reported. An endoscopic manipulator has been produced by Rose *et al.*[6] This manipulator utilizes a parallel kinematic mechanism. However, the largest bending angle of the manipulator is not equal in every direction because of the distinctive design of its limbs. This manipulator can accomplish ±80° in one direction and ±40° in the perpendicular direction. Nonetheless, the kinematics analysis of this mechanism is exceptionally troublesome and has not been reported. Ibrahim *et al.*[7] have proposed a 4-DOF parallel manipulator (2-PUU_2-PUS). A real prototype of this 4-DOF parallel manipulator was produced from annealed stainless steel.[8] Singularity problems for this 4-DOF parallel manipulator are reported by Khalifa *et al.*[9] Modification of the design of this manipulator is necessary to overcome these problems.

Parallel tool heads that possess 2R1T degrees of freedom have turned out to be critical in the field of machine tools. Parallel manipulators that possess 2R1T DOFs have been developed and studied in recent decades. The 3-PRS manipulator is the most well-known architecture.[10] This parallel manipulator consists of three limbs (each limb consists of one active prismatic joint (P), one passive revolute joint (R) and one passive spherical joint (S)). This manipulator needs precise spherical joints, which are troublesome and costly to fabricate. For that reason, this manipulator has not achieved great advances and applications up to this point.

In this article, a new dexterous endoscopic manipulator for minimally invasive surgery (MIS) is proposed. This novel surgical robot is based on a parallel manipulator with 3-PUU architecture that has 2R1T DOFs. Moreover, the proposed endoscopic parallel manipulator has the ability to achieve a bending angle of more than ±90° in any direction. Unlike the 3-PRS mechanism, the proposed 3-PUU surgical robot does not need precise spherical joints. Hence, from the practical viewpoint, the 3-PUU manipulator has the best orientation capability. Also, it is cheaper and easier to produce than other designs.

It is worth mentioning that some 3-PUU parallel manipulators already exist.[11,12] All these 3-PUU manipulators except Liping's have three pure translational (3T) DOFs. Liping's manipulator[12] has 2R1T DOFs so it can be utilized as an orientation mechanism. The major drawback of Liping's manipulator is that its bending angle cannot exceed 58° in any direction. On the other hand, the 3-PUU surgical manipulator proposed in this work possesses 2R1T DOFs and it is able to perform the orientation task perfectly. Its bending angle can reach more than ±90° in any direction. The minor distinction in the arrangement of the joints' axes in these sorts of 3-PUU manipulators leads to great differences between their motions. The proposed manipulator possesses a new arrangement of the joints' axes, which endows it with superior characteristics. On the other hand, it has an uncommon wrench system of h-pitch. This type of wrench system is usually avoided in the literature because of its complicated mathematical analysis. Most previous parallel manipulators have wrench systems with either zero pitch or infinite pitch, which are easier to analyse. Therefore, a geometrical/analytical approach is used to facilitate the kinematic analysis of PMs with h-pitch wrench systems.

This paper is organized as follows. The description of the slave surgical manipulator is presented in Section 2. Section 3 describes the differences from previous systems. Inverse kinematics analysis of the proposed parallel manipulator is introduced in Section 4, and forward kinematics analysis of it is described in Section 5. A geometrical/analytical approach for reciprocal screw-based singularity analysis of 3-PUU is presented in Section 6. Section 7 discusses the singular configurations of the proposed 3-PUU PM. In Section 8, evaluation for the workspace of the proposed 3-PUU PM is described. The experimental setup and system verification are introduced in Section 9. Finally, conclusions and future work are summarized in Section 10.

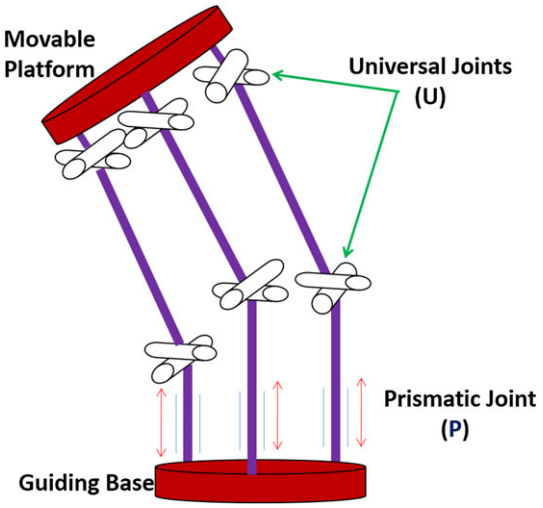

FIGURE 1 Schematic diagram of the proposed parallel manipulator (3-PUU)

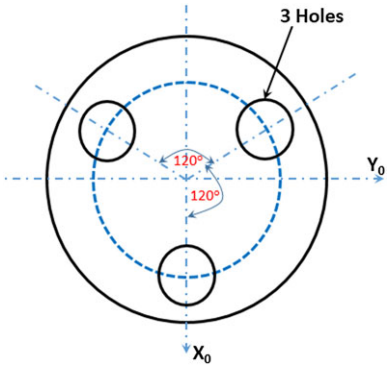

FIGURE 2 Schematic diagram of the guiding base platform

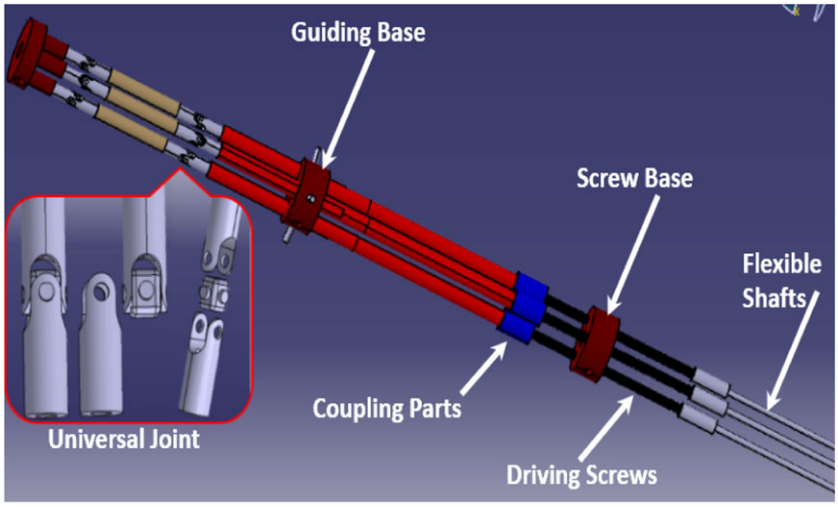

FIGURE 3 CAD model of the proposed parallel manipulator (3-PUU)

2 | DESCRIPTION OF THE PROPOSED MANIPULATOR

A schematic diagram of the proposed 3-PUU parallel manipulator is illustrated in Figure 1. Figure 2 shows a schematic diagram of the fixed guiding base. This proposed manipulator consists of 3 limbs that have a unique arrangement of joints connecting the fixed platform with the movable one. The 3 limbs have identical kinematic structure. Each limb has 2 links and 3 joints (1 prismatic and 2 universal joints). The first joints in the 3 limbs that connect the fixed base with the first links in the limbs are prismatic joints with parallel axes. The 3 axes of the prismatic joints are arranged symmetrically on the perimeter of a circle that is perpendicular to these axes. The first axis of the first universal joint in each limb is perpendicular to the plane formed by the axis of the limb's prismatic joint and the centre of the circle mentioned above. In each limb, the second axis of the first universal joint and the first axis of the second universal joint are parallel to each other and perpendicular to the line connecting the centres of the 2 universal joints.

The computer aided design (CAD) model of the proposed 3-PUU parallel manipulator is presented in Figure 3. A screw is used to convert the rotary motion of the motor into linear motion, which will be used to actuate the prismatic joint. The actuators (rotary motors) are positioned outside the human body and transmit power to the proposed manipulator by rotating flexible shafts, which control the motion of the prismatic joints. A flexible shaft (flexible tube) bends easily and provides a flexible path for this power transmission. By rotating the motor, the driving screw will rotate via rotation of the flexible shaft, which has rather large torsional stiffness. The driving screw engages with its nut, which is bored in the screw base as shown in Figure 3. The screw base is fixed with a cylindrical cover by fixation screws. The cylindrical cover will be attached to a holder unit, which is clamped to a rigid frame above the patient. This holder unit is used for positioning the proposed manipulator (3-PUU) inside the patient's body and providing any required coarse motion.

The driving screw will rotate and move up and down relative to the fixed screw base, according to the direction of rotation of the motor as shown in Figure 4. For proper working of the prismatic link, it must be constrained from rotation with the screw. The driving screw tip, shown in Figure 5, is attached to the prismatic link with a connection that permits the translational motion of the driving screw to be transmitted without its rotational motion. This is achieved by making a hole in the lower end of the prismatic link as shown in Figure 5. The diameter of this hole is a bit larger than the diameter of the screw tip that is placed inside this hole. The coupling part is a hollow cylinder with a lower base that

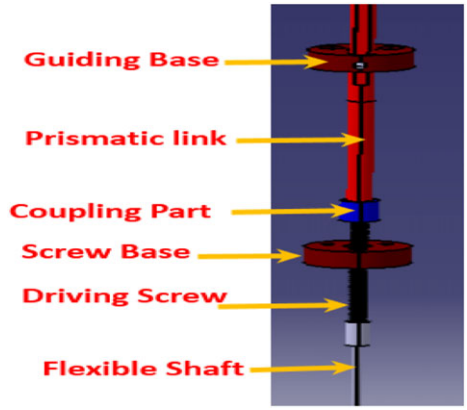

FIGURE 4 CAD model of the transmission of the first joint

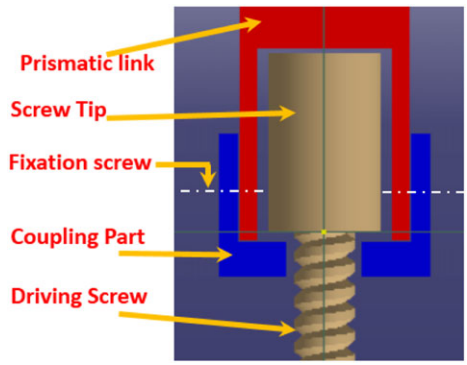

FIGURE 5 CAD model of the coupling system

has a central hole. This central hole has a diameter larger than the diameter of the driving screw and less than the diameter of the cylindrical screw tip. The coupling part is rigidly fixed to the prismatic link by fixation screws and locking devices. When the driving screw moves upward, it will push the prismatic link in the same direction without forcing it to rotate. When the driving screw moves downward, it will push the coupling part and consequently the prismatic link downward without forcing the rotational motion to be transmitted. To prevent the rotation of the prismatic link, a guiding base is used as shown in Figures 4 and 6. This guiding base is rigidly attached to the fixed cylindrical cover by a fixation screw. A groove is made in the prismatic link, which goes through a hole in the guiding base as shown in Figure 6. Rotational motion is prevented by a set screw whose tip is placed inside the groove, and its body is engaged with a nut bored in the body of the guiding base as shown in Figure 6. This set screw is delivered to its location through a hole in the fixed cylindrical cover.

By inhibiting rotation of the prismatic link, linear motion is accomplished as the motor turns. The precision of linear motion depends on the pitch of the driving screw and the resolution of the motor driving system. A control system will be used to control the actuators in order to perform a certain motion of the movable platform with high accuracy. A surgical tool will be attached to the centre of the movable platform. A central hole is made in the guiding base and in the screw base to permit any wiring connection needed for the surgical tool.

The virtual prototype is constructed using ADAMS software in order to validate the proposed manipulator and its bending capability. The validation results are shown in Figure 7. These results indicate the ability of the proposed manipulator (3-PUU) to bend in any direction with a large bending angle that can exceed ±90°.

3 | DIFFERENCES FROM PREVIOUS SYSTEMS

The principal difference between the proposed 3-PUU parallel manipulator represented in Figures 1 and 2 and the 3-PUU manipulator produced by Tsai[11] lies in the arrangement of the prismatic joints. The prismatic joints' axes that are presented in Figures 1 and 2 are parallel to each other and are not contained in the same plane. Tsai has proposed 2 architectures for 3-PUU with 3 translational DOFs. In the first architecture, the prismatic joints' axes intersect at a common point; in the second one, these axes are parallel to each other and are contained in the same plane. Hence, a considerable difference between DOFs' characteristics arises due to the difference in the arrangement of the prismatic joints' axes. Our proposed manipulator has 2R1T DOFs so it can be utilized as an orientation mechanism, in contrast to Tsai's manipulators, which are used as position mechanisms.

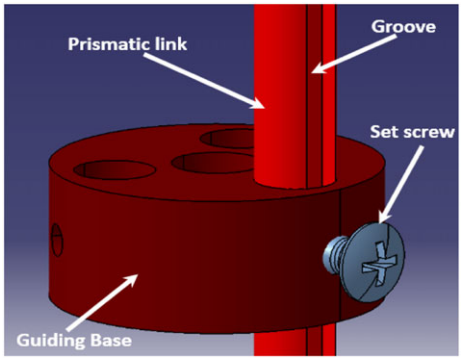

FIGURE 6 CAD model of the prismatic joint (P)

The principal difference between the proposed 3-PUU parallel manipulator represented in Figures 1 and 2 and the 3-PUU manipulator produced by Liping *et al.*[12] lies in the arrangement of the universal joints' axes. In each limb of Liping's manipulator, the first axis of the first universal joint is parallel to the axis of the prismatic joint, while in our manipulator this axis is normal to it. The two manipulators differ in their motion features. The proposed manipulator has 2R1T DOFs, and the bending angle can exceed 90° in any direction. Liping's manipulator also has 2R1T DOFs, but the bending angle cannot exceed 58° in any direction. This can be attributed to the wrench system of the moving platform. The wrench system in the proposed manipulator has h-pitch, while in Liping's manipulator it has zero pitch.

THe 2-PUU_2-PUS manipulator introduced by Khalil *et al.*[7,8] has 4-DOF and can be used as an orientation mechanism. This manipulator consists of 4 limbs. Each pair of opposite limbs has the same structure, which leads to the existence of many configurations with dependent wrenches and consequently a workspace with interior singularities. Singularity problems for this 4-DOF parallel manipulator are reported by Khalifa *et al.*[9] The proposed manipulator (3-PUU) consists of 3 limbs arranged symmetrically on the perimeter of a circle, which prevents the dependency of the wrenches and consequently provides a workspace almost free from interior singularities.

4 | INVERSE KINEMATICS ANALYSIS OF THE 3-PUU PM

For inverse kinematics, the position vector $\boldsymbol{P}_c$ of a point c located at the centre of the movable platform and the rotation matrix ${}^{b}\boldsymbol{R}_m$ of the movable platform are given, and the problem is to find the linear displacements of the input prismatic joints. As mentioned in section 2, the prismatic joints' axes are parallel to each other and arranged symmetrically on the perimeter of a circle with radius *r*. Henceforward, this circle is assumed to be located on the upper surface of the guiding base disc. A fixed Cartesian frame O-*XYZ* is attached to the centre of this circle. The *X*-axis of the fixed Cartesian frame O-*XYZ* is located in the plane of the circle and directed from the centre of the circle to the first prismatic joint axis. The *Z*-axis is normal to the plane of the circle and passes through its centre. The *Y*-axis satisfies the right-hand rule. A body frame C-*UVW*, which possesses the same pose as the fixed frame O-*XYZ*, is attached to the centre of the movable platform. Figure 8 shows the vector representation of the kinematic chains of the parallel manipulator 3-PUU. Points $\boldsymbol{A}_i$ and $\boldsymbol{B}_i$ (for $i = 1, 2$ and 3) represent the location of the first and second universal joints in the *i*th limb, respectively. Points $\boldsymbol{P}_i$ represent the intersection point between the prismatic joint axis in the *i*th limb and the plane of the circle. Input links $\boldsymbol{P}_i\boldsymbol{A}_i$ have variable lengths

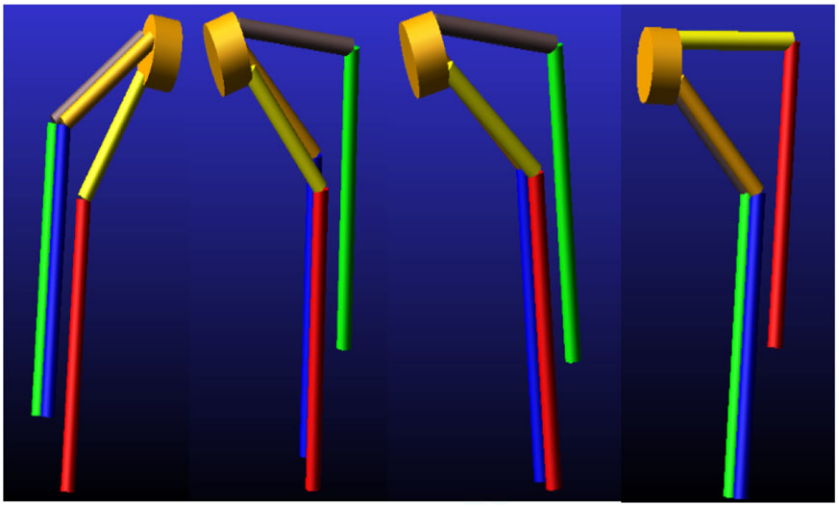

FIGURE 7 Different bending angle configurations of the 3-PUU parallel manipulator

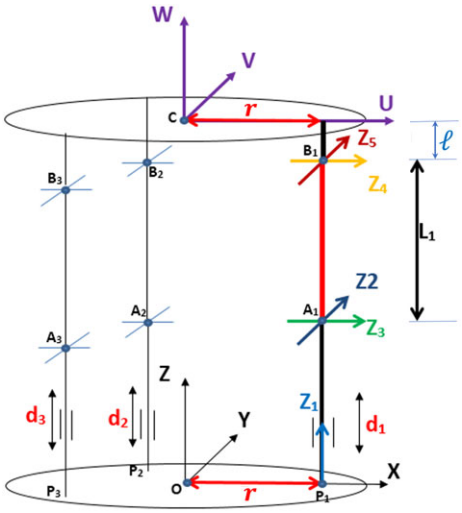

FIGURE 8 Schematic diagram of the kinematic chains in the proposed manipulator (3-PUU)

d_i in the Z-direction as a result of the movements of the actuators, while links $\boldsymbol{A_iB_i}$ have fixed length L_i. With respect to the fixed reference frame O-XYZ, the coordinates of points $\boldsymbol{P_i}$ are given by

$$\boldsymbol{P_1} = \begin{bmatrix} r \\ 0 \\ 0 \end{bmatrix}, \quad \boldsymbol{P_2} = \begin{bmatrix} r\cos(2\pi/3) \\ r\sin(2\pi/3) \\ 0 \end{bmatrix}, \quad \boldsymbol{P_3} = \begin{bmatrix} r\cos(4\pi/3) \\ r\sin(4\pi/3) \\ 0 \end{bmatrix}. \tag{1}$$

Moreover, coordinates of points $\boldsymbol{A_i}$ are given by

$$\boldsymbol{A_i} = \boldsymbol{P_i} + \begin{bmatrix} 0, & 0, & d_i \end{bmatrix}^T \quad \text{for } i = 1, 2, 3. \tag{2}$$

Similarly, the coordinates of points $\boldsymbol{B_i}$ with respect to the body frame C-UVW are denoted as ${}^m\boldsymbol{B_i}$ and are given by

$${}^m\boldsymbol{B_1} = \begin{bmatrix} r \\ 0 \\ -\ell \end{bmatrix}, \quad {}^m\boldsymbol{B_2} = \begin{bmatrix} r\cos(2\pi/3) \\ r\sin(2\pi/3) \\ -\ell \end{bmatrix}, \quad {}^m\boldsymbol{B_3} = \begin{bmatrix} r\cos(4\pi/3) \\ r\sin(4\pi/3) \\ -\ell \end{bmatrix}, \tag{3}$$

where ℓ is the offset between the centre of the second universal joint, in any limb, and the UV plane. With respect to the fixed frame O-XYZ, the coordinates of points $\boldsymbol{B_i}$ are calculated according to

$$\boldsymbol{B_i} = {}^b\boldsymbol{R_m}.{}^m\boldsymbol{B_i} + \boldsymbol{P_c}. \tag{4}$$

For each elementary serial chain, the kinematic closure can be provided as

$$\|\boldsymbol{A_iB_i}\|^2 = L_i^2. \tag{5}$$

Using Figure 9, it is simpler to write

$$\boldsymbol{A_iB_i} = \boldsymbol{e_i} - d_i.\boldsymbol{Z}, \tag{6}$$

where $\boldsymbol{Z}$ is a unit vector in the Z-direction. Also, $\boldsymbol{e_i}$ can be calculated from

$$\boldsymbol{e_i} = {}^b\boldsymbol{R_m}.{}^m\boldsymbol{B_i} + \boldsymbol{P_c} - \boldsymbol{P_i}. \tag{7}$$

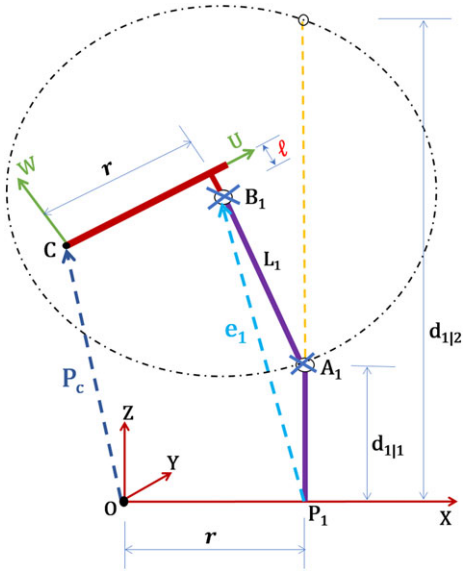

FIGURE 9 Schematic diagram of the first kinematic chain in the proposed manipulator

Substitution of equation (6) into equation (5) yields

$$\|\boldsymbol{A_iB_i}\|^2 = \boldsymbol{e_i}^2 + d_i^2 - 2\boldsymbol{e_i}\cdot d_i\cdot \boldsymbol{Z} = L_i^2. \quad (8)$$

The two solutions of equation 8 can be represented in a simple form as

$$d_{i|1,2} = \boldsymbol{e_i}\cdot \boldsymbol{Z} \pm \sqrt{(\boldsymbol{e_i}\cdot \boldsymbol{Z})^2 - \boldsymbol{e_i}^{\mathrm{T}}\cdot \boldsymbol{e_i} + L_i^2}. \quad (9)$$

Equation 9 demonstrates that there are two solutions for the displacement of the actuators representing the intersection between the displacement vector $d_i \cdot \boldsymbol{Z}$ and the surface of a sphere as shown in Figure 9. This sphere has radius L_i, and its centre is located at $\boldsymbol{B_i}$. The negative sign of the square root, which represents the lower intersection point, is selected in order to minimize the displacement of actuators. Hence, the closed-form solution for the inverse kinematics of the parallel manipulator (3-PUU) is represented in equation 9 by taking the negative sign only.

5 | FORWARD KINEMATICS ANALYSIS OF 3-PUU PM

For the 3-PUU parallel manipulator, supposing that d_1, d_2 and d_3 are known, we can solve for the values of $\boldsymbol{P_c}$ and ${}^b\boldsymbol{R_m}$. They can be calculated using the kinematics of each limb individually. Let us assume that $\boldsymbol{P_{ci}}$ and ${}^b\boldsymbol{R_{mi}}$ respectively represent the position vector and rotation matrix of the movable platform according to the *i*th limb,. Consequently, each limb provides us with two expressions representing the position vector and the rotation matrix of the movable platform. The kinematic closure of the first chain (PUU) can be written as

$${}^b\boldsymbol{R_{m1}} = \boldsymbol{R_y}(\alpha_1)\cdot \boldsymbol{R_x}(\beta_1)\cdot \boldsymbol{R_x}(\gamma_1)\cdot \boldsymbol{R_y}(\delta_1), \quad (10)$$

$$\boldsymbol{P_{c1}} = \boldsymbol{A_1} + \boldsymbol{R_y}(\alpha_1)\cdot \boldsymbol{R_x}(\beta_1)\cdot L_1\boldsymbol{Z} - {}^b\boldsymbol{R_{m1}}\cdot {}^m\boldsymbol{B_1}, \quad (11)$$

where α_i and β_i are the two angles of the first universal joint in the *i*th limb for $i = 1, 2$ and 3. Also, γ_i and δ_i are the two angles of the second universal joint in the *i*th limb. Moreover, $\boldsymbol{R}_{\cdot}(*)$ is a rotation matrix representing a rotation of angle (*) about axis (.). See[13] for the definition of the rotation matrix. Similarly, the two expressions for the second chain PUU can be written as

$${}^b\boldsymbol{R_{m2}} = \boldsymbol{R_z}(-\pi/3)\cdot \boldsymbol{R_y}(\alpha_2)\cdot \boldsymbol{R_x}(\beta_2)\cdot \boldsymbol{R_x}(\gamma_2)\cdot \boldsymbol{R_y}(\delta_2)\cdot \boldsymbol{R_z}(\pi/3), \quad (12)$$

$$\boldsymbol{P_{c2}} = \boldsymbol{A_2} + \boldsymbol{R_z}(-\pi/3)\cdot \boldsymbol{R_y}(\alpha_2)\cdot \boldsymbol{R_x}(\beta_2)\cdot L_2\boldsymbol{Z} - {}^b\boldsymbol{R_{m2}}\cdot {}^m\boldsymbol{B_2}. \quad (13)$$

Similarly, the two expressions for the third chain PUU can be provided as

$${}^b\boldsymbol{R_{m3}} = \boldsymbol{R_z}(\pi/3)\cdot \boldsymbol{R_y}(\alpha_3)\cdot \boldsymbol{R_x}(\beta_3)\cdot \boldsymbol{R_x}(\gamma_3)\cdot \boldsymbol{R_y}(\delta_3)\cdot \boldsymbol{R_z}(-\pi/3), \quad (14)$$

$$\boldsymbol{P_{c3}} = \boldsymbol{A_3} + \boldsymbol{R_z}(\pi/3)\cdot \boldsymbol{R_y}(\alpha_3)\cdot \boldsymbol{R_x}(\beta_3)\cdot L_3\boldsymbol{Z} - {}^b\boldsymbol{R_{m3}}\cdot {}^m\boldsymbol{B_3}. \quad (15)$$

By equating the position (rotation matrix) resulting from a certain limb with the position (rotation matrix) resulting from the other 2 limbs, 12 equations will be obtained according to the following procedure:

1. Equate $\boldsymbol{P_{c1}}$ in equation 11 and $\boldsymbol{P_{c2}}$ in equation 13.
2. Equate $\boldsymbol{P_{c1}}$ in equation 11 and $\boldsymbol{P_{c3}}$ in equation 15.
3. Equate ${}^b\boldsymbol{R_{m1}}$ in equation 10 and ${}^b\boldsymbol{R_{m2}}$ in equation 12.
4. Equate ${}^b\boldsymbol{R_{m1}}$ in equation 10 and ${}^b\boldsymbol{R_{m3}}$ in equation 14.

The resulting equations could be solved using a MATLAB program. It is clear that from these 12 nonlinear equations, we can obtain 12 unknown variables ($\alpha_i, \beta_i, \gamma_i, \delta_i; i = 1, 2, 3$). Finally, the forward kinematics can be solved by substituting the passive joints' values of the first limb ($\alpha_1, \beta_1, \gamma_1, \delta_1$) into equations 10 and 11, and therefore $\boldsymbol{P_c}$ and ${}^b\boldsymbol{R_m}$ can be obtained.

According to the forward kinematics analysis of the proposed PM, the reachable workspace can be determined numerically, considering the angle limitation of the universal joint, as presented in Figure 10. In finding the whole workspace, all the mechanical limits of the prismatic and universal joints were taken into consideration. For the prismatic

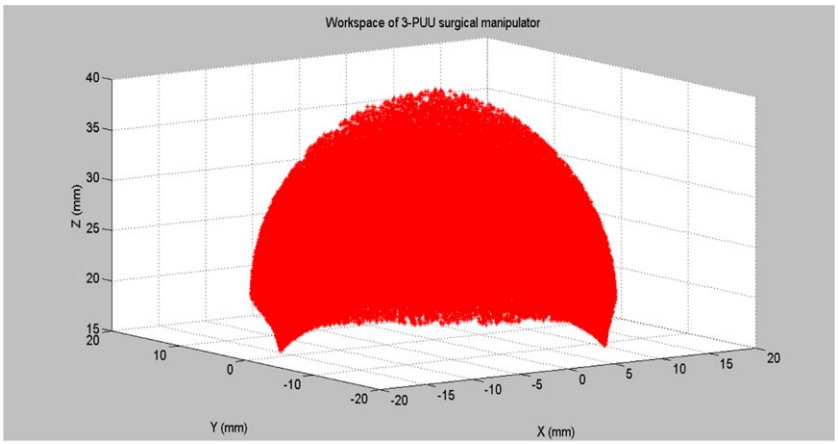

FIGURE 10 Workspace of the 3-PUU parallel manipulator

joint, we take into account the length of its stroke. As stated by the manufacturers of the small-scale universal joint of the type MAAS 1.0,[14] the angle limitation is ±90° for one angle and ±30° for the other angle, i.e. the sum of the two angles is less than or equal to 120°.

6 | GEOMETRICAL/ANALYTICAL APPROACH FOR RECIPROCAL SCREW-BASED SINGULARITY ANALYSIS OF THE 3-PUU

The proposed manipulator 3-PUU has a new arrangement of the joints' axes, which endows it with superior characteristics. However, it has an uncommon wrench system of h-pitch. This type of wrench system is usually avoided in the literature due to its complicated mathematical analysis. Most previous parallel manipulators have wrench systems with either zero pitch or infinite pitch, which are easier to analyse. A reciprocal screw of zero pitch means that the movable platform is constrained by a pure force. On the other hand, a reciprocal screw of infinite pitch means that the movable platform is constrained by a pure couple. A reciprocal screw of h-pitch means that the movable platform is constrained by a combination of forces and couples that have a certain relationship. It is not possible to find out the singular configurations geometrically in such cases since a reciprocal screw of h-pitch changes its pitch value with a change in its configuration. Therefore, a geometrical/analytical approach is developed to facilitate the singularity analysis of PMs with h-pitch wrench systems.[9] This algorithm will be applied for the proposed 3-PUU PM in this section.

At the beginning, all the joints of the manipulator can be reduced to simple prismatic or revolute joints. So, the wrench system of each joint consists of screws of zero and/or infinity pitch. The wrench system of the movable platform is the linear combination of the wrench systems of all limbs while the wrench system of each limb is the intersection of the wrench systems of the joints in this limb. The h-pitch wrench systems may appear during the process of intersection or linear combination. The geometrical approach is used until the point where an h-pitch screw appears. At this point, the analytical approach is applied. The analytical approach is used to express the 6 components of the resulting h-pitch reciprocal screw as functions of the configuration parameters. Comparing the analytical expressions of different h-pitch reciprocal screws reveals simple geometrical conditions in which a linear dependence between these reciprocal screws occurs and hence a singularity. These simple geometrical conditions will guide the numerical search to find all the singular configurations in a simple and efficient manner.

In the following, the unit screws associated with all joints' axes in the limb will be calculated. Then, the reciprocal screws will be found both with the actuators locked and without locking them. These calculations will be performed for each limb individually. All these reciprocal screws will be used in constructing the Jacobian matrix, and evaluating the workspace in the following sections. As the three limbs have identical kinematic structure, the mathematical derivation is the same for each limb. The mathematical derivation of the first limb is introduced in more detail as follows.

The first limb connects the fixed guiding base to the movable platform by a prismatic joint, followed by two universal joints (PUU) as illustrated in Figure 8. The position vector of the second universal joint, point $\boldsymbol{B_1}$ with respect to O-*XYZ*, can be described as

$$\boldsymbol{B_1} = \boldsymbol{A_1} + \boldsymbol{R}_y(\alpha_1)\cdot\boldsymbol{R}_x(\beta_1)\cdot\begin{bmatrix}0\\0\\L_1\end{bmatrix} = \begin{bmatrix} r + L_1\sin(\alpha_1)\cos(\beta_1)\\ -L_1\sin(\beta_1)\\ d_1 + L_1\cos(\alpha_1)\cos(\beta_1)\end{bmatrix}. \quad (16)$$

The universal joint can be replaced by two intersecting revolute joints. So, the i^{th} limb may be considered as a serial chain connecting the movable platform to the fixed base by five 1-DOF joints. Let $\boldsymbol{s}_{j,i}$ be a unit vector along the *j*th joint axis of the *i*th limb (for $i = 1, 2, 3; j = 1, 2, \dots, 5$). Now, we will calculate the unit vector associated with all joints' axes in the first limb as shown in Figure 8. The fixed frame O-*XYZ* is chosen to be the reference frame at which all the screws are expressed.

$$\boldsymbol{s}_{1,1} = \begin{bmatrix}0,\ 0,\ 1\end{bmatrix}^T, \qquad \boldsymbol{s}_{2,1} = \begin{bmatrix}0,\ 1,\ 0\end{bmatrix}^T, \quad (17)$$

$$\boldsymbol{s}_{3,1} = \boldsymbol{R}_y(\alpha_1)\cdot\begin{bmatrix}1,\ 0,\ 0\end{bmatrix}^T = \begin{bmatrix}\cos(\alpha_1),\ 0, -\sin(\alpha_1)\end{bmatrix}^T, \quad (18)$$

$$\boldsymbol{s}_{4,1} = \boldsymbol{R}_y(\alpha_1)\cdot\boldsymbol{R}_x(\beta_1)\cdot\begin{bmatrix}1,\ 0,\ 0\end{bmatrix}^T = \begin{bmatrix}\cos(\alpha_1),\ 0, -\sin(\alpha_1)\end{bmatrix}^T, \quad (19)$$

$$\boldsymbol{s}_{5,1} = \boldsymbol{R}_y(\alpha_1)\cdot\boldsymbol{R}_x(\beta_1)\cdot\boldsymbol{R}_x(\gamma_1)\cdot\begin{bmatrix}0\\1\\0\end{bmatrix} = \begin{bmatrix}\sin(\alpha_1)\sin(\beta_1+\gamma_1)\\ \cos(\beta_1+\gamma_1)\\ \cos(\alpha_1)\sin(\beta_1+\gamma_1)\end{bmatrix}. \quad (20)$$

For the prismatic joint, the pitch of the twist screw will be infinite, and the unit screw is reduced to

$$\hat{\$}_{1,1} = \begin{bmatrix}[\boldsymbol{0}]_{3\times1}\\ \boldsymbol{s}_{1,1}\end{bmatrix}. \quad (21)$$

As mentioned before, the universal joint can be replaced by two intersecting revolute joints. For the revolute joint, the pitch of the screw will be zero, and the unit screw is calculated as

$$\hat{\$}_{k,1} = \begin{bmatrix}\boldsymbol{s}_{k,1}\\ \boldsymbol{s}_{0k,1}\times\boldsymbol{s}_{k,1}\end{bmatrix} \qquad \text{for } k = 2, 3, 4, 5. \quad (22)$$

Moreover, $\boldsymbol{s}_{0k,1}$ is the position vector of a point existing on the screw axis, and it is found to be

$$\boldsymbol{s}_{0k,1} = \begin{cases}\boldsymbol{A_1} & \text{for } k = 2, 3.\\ \boldsymbol{B_1} & \text{for } k = 4, 5.\end{cases} \quad (23)$$

With the actuator locked, the connectivity of the first limb is equal to 4. The reciprocal screws for this limb, which is reciprocal to all the passive joint screws, form a 2-system. One screw, $\hat{\$}_{r1,1}$, can be readily identified as a zero-pitch screw along the line passing through the two centres of the two universal joints. The second screw, $\hat{\$}_{r2,1}$, which is also reciprocal to all the passive joint screws, can be readily identified as a zero-pitch screw along the intersection line of two planes as shown in Figure 11. The first plane contains the two axes of the first universal joint and the second plane contains the two axes of the second universal joint.

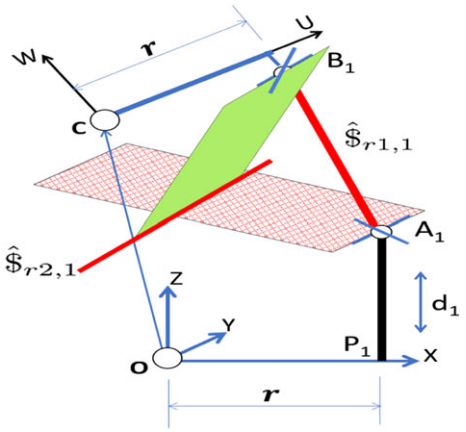

FIGURE 11 Reciprocal screws of the first limb PUU

Without locking the prismatic joint, the connectivity of the first limb is equal to 5. Hence, the reciprocal screws for this limb form a 1-system, which is a screw that is reciprocal to all the joint screws of the first limb. This reciprocal screw, $\hat{\$}_{rt,1}$, is a linear combination between $\hat{\$}_{r1,1}$ and $\hat{\$}_{r2,1}$ and must satisfy the reciprocal condition with the prismatic joint screw. Here, the h-pitch reciprocal screw $\hat{\$}_{rt,1}$ will appear due to the linear combination of $\hat{\$}_{r1,1}$ and $\hat{\$}_{r2,1}$, whose axes are non-parallel non-intersecting lines. So, the geometrical approach is stopped and the analytical approach will be used to express the 6 components of the resulting h-pitch reciprocal screw as functions of the configuration parameters. Actually, to get an analytical expression for $\hat{\$}_{rt,1}$, analytical expressions for $\hat{\$}_{r1,1}$ and $\hat{\$}_{r2,1}$ need to be calculated first.

In the following, these reciprocal screws are calculated analytically. Concerning the first reciprocal screw, let $\boldsymbol{s}_{r1,1}$ be a unit vector along the line passing through the two centres of the two universal joints. $\boldsymbol{s}_{r1,1}$ can be identified easily from

$$\boldsymbol{s}_{r1,1} = \boldsymbol{R}_y(\alpha_1)\cdot\boldsymbol{R}_x(\beta_1)\cdot\begin{bmatrix}0\\0\\1\end{bmatrix} = \begin{bmatrix}\sin(\alpha_1)\cos(\beta_1)\\-\sin(\beta_1)\\\cos(\alpha_1)\cos(\beta_1)\end{bmatrix}. \tag{24}$$

Furthermore, $\boldsymbol{s}_{r01,1}$ is a vector from the origin of the reference frame to a point that existed on the line passing through the two centres of the two universal joints, which can be calculated easily from $\boldsymbol{s}_{r01,1} = \boldsymbol{A}_1$. Knowing $\boldsymbol{s}_{r1,1}$ and $\boldsymbol{s}_{r01,1}$, a zero-pitch screw $\hat{\$}_{r1,1}$ can be identified as

$$\hat{\$}_{r1,1} = \begin{bmatrix}\sin(\alpha_1)\cos(\beta_1)\\-\sin(\beta_1)\\\cos(\alpha_1)\cos(\beta_1)\\d_1\sin(\beta_1)\\d_1\sin(\alpha_1)\cos(\beta_1) - r\cos(\alpha_1)\cos(\beta_1)\\-r\sin(\beta_1)\end{bmatrix}. \tag{25}$$

Concerning the second reciprocal screw, the equation of the first plane can be given as

$$-\sin(\alpha_1)X - \cos(\alpha_1)Z = dp_{1,1}, \tag{26}$$

where $dp_{1,1} = -r\sin(\alpha_1) - d_1\cos(\alpha_1)$.

Also, the equation of the second plane can be provided as

$$\sin(\alpha_1)\cos(\beta_1+\gamma_1)X - \sin(\beta_1+\gamma_1)Y + \cos(\alpha_1)\cos(\beta_1+\gamma_1)Z = dp_{2,1}, \tag{27}$$

where $dp_{2,1} = L_1\sin(\beta_1+\gamma_1)\sin(\beta_1) + \cos(\beta_1+\gamma_1)\cos(\alpha_1)[d_1 + L_1\cos(\alpha_1)\cos(\beta_1)] + \cos(\beta_1+\gamma_1)\sin(\alpha_1)[r + L_1\sin(\alpha_1)\cos(\beta_1)]$.

A unit vector $\boldsymbol{s}_{r2,1}$ that lies on the intersection line of the two planes can be provided as

$$\boldsymbol{s}_{r2,1} = \left[-\cos(\alpha_1),\ 0,\ \sin(\alpha_1)\right]^T. \tag{28}$$

In order to completely identify the second reciprocal screw $\hat{\$}_{r2,1}$, a point existing on the two planes needs to be found. This point is obtained by solving the two equations of the two planes together. Then, $\hat{\$}_{r2,1}$ can be identified as a zero-pitch screw along the intersection line between the two planes, and it is calculated as

$$\hat{\$}_{r2,1} = \begin{bmatrix}-\cos(\alpha_1)\\0\\\sin(\alpha_1)\\-L_1\sin(\alpha_1)\cos(\gamma_1)/\sin(\beta_1+\gamma_1)\\-d_1\cos(\alpha_1) - r\sin(\alpha_1)\\-L_1\cos(\alpha_1)\cos(\gamma_1)/\sin(\beta_1+\gamma_1)\end{bmatrix}. \tag{29}$$

Without locking the prismatic joint, the reciprocal screw $\hat{\$}_{rt,1}$ is a linear combination between $\hat{\$}_{r1,1}$ and $\hat{\$}_{r2,1}$ that must satisfy the reciprocal condition with the prismatic joint screw. This linear combination is provided as

$$\hat{\$}_{rt,1} = \frac{a_1}{\sqrt{a_1^2+b_1^2}}\hat{\$}_{r1,1} + \frac{b_1}{\sqrt{a_1^2+b_1^2}}\hat{\$}_{r2,1}, \tag{30}$$

where a_1 and b_1 are unknown numbers that satisfy the equation. In the above linear combination, the term $\sqrt{a_1^2+b_1^2}$ is used to get a unit reciprocal screw. Furthermore, the general form of the reciprocal screw is expressed as

$$\hat{\$}_{rt,1} = \begin{bmatrix}\boldsymbol{s}_{rt,1}\\\boldsymbol{s}_{0rt,1}\times\boldsymbol{s}_{rt,1} + \lambda_1\cdot\boldsymbol{s}_{rt,1}\end{bmatrix}, \tag{31}$$

where $\boldsymbol{s}_{rt,1}$ is a unit vector along the axis of the reciprocal screw $\hat{\$}_{rt,1}$ that is reciprocal to all the joints' screws of the first limb. Also, $\boldsymbol{s}_{0rt,1}$ refers to the vector from the origin of the reference frame to any point existing on the axis of the reciprocal screw $\hat{\$}_{rt,1}$. Moreover, λ_1 represents the pitch of the reciprocal screw $\hat{\$}_{rt,1}$. Using equations 25, 29, 30 and 31, it is concluded that

$$\boldsymbol{s}_{rt,1} = \frac{a_1}{\sqrt{a_1^2+b_1^2}}\begin{bmatrix}\sin(\alpha_1)\cos(\beta_1)\\-\sin(\beta_1)\\\cos(\alpha_1)\cos(\beta_1)\end{bmatrix} + \frac{b_1}{\sqrt{a_1^2+b_1^2}}\begin{bmatrix}-\cos(\alpha_1)\\0\\\sin(\alpha_1)\end{bmatrix}. \tag{32}$$

This reciprocal screw $\hat{\$}_{rt,1}$ must be reciprocal with the prismatic joint screw $\hat{\$}_{1,1}$ provided in equation 21. This condition can be written as

$$\boldsymbol{s}_{rt,1}^{\mathrm{T}}\cdot\boldsymbol{s}_{1,1} = 0. \tag{33}$$

The previous equation will lead to

$$\frac{a_1}{\sqrt{a_1^2+b_1^2}}\cos(\alpha_1)\cos(\beta_1) + \frac{b_1}{\sqrt{a_1^2+b_1^2}}\sin(\alpha_1) = 0. \tag{34}$$

Then, find an expression for a_1 as a function of b_1 such as

$$a_1 = \frac{-b_1\sin(\alpha_1)}{\cos(\alpha_1)\cos(\beta_1)}. \tag{35}$$

Using Eqs. 25, 29, 30 and 35, $\hat{\$}_{rt,1}$ and λ_1 can be expressed as

$$\hat{\$}_{rt,1} = \frac{1}{\sin(\beta_1+\gamma_1)\sqrt{\cos^2(\alpha_1)\cos^2(\beta_1)-\cos^2(\alpha_1)+1}} \begin{bmatrix} r11 \\ r12 \\ r13 \\ r14 \\ r15 \\ r16 \end{bmatrix}, \quad (36)$$

where

$$r_{11} = -\cos(\beta_1)\sin(\beta_1+\gamma_1),$$
$$r_{12} = \sin(\alpha_1)\sin(\beta_1)\sin(\beta_1+\gamma_1),$$
$$r_{13} = 0,$$
$$r_{14} = -\sin(\alpha_1)[d_1\sin(\beta_1+\gamma_1)\sin(\beta_1)+L_1\cos(\alpha_1)\cos(\beta_1)\cos(\gamma_1)],$$
$$r_{15} = -d_1\cos(\beta_1)\sin(\beta_1+\gamma_1),$$
$$r_{16} = -[L_1\cos^2(\alpha_1)\cos(\beta_1)\cos(\gamma_1) - r\sin(\beta_1+\gamma_1)\sin(\alpha_1)\sin(\beta_1)].$$

$$\lambda_1 = \frac{L_1\cos(\alpha_1)\cos^2(\beta_1)\cos(\gamma_1)\sin(\alpha_1)}{\sin(\beta_1+\gamma_1)[\cos^2(\alpha_1)\cos^2(\beta_1)-\cos^2(\alpha_1)+1]}. \quad (37)$$

It is clear that the pitch of the reciprocal screw λ_1 depends on the configuration because it is a function of the angles of the two universal joints.

It is worth mentioning that there is a special case when the two planes (each plane contains the two axes of a universal joint) are parallel to each other. In this case, there is no intersection line between the two planes, hence $\hat{\$}_{r2,1}$ could not be obtained by the above method. In this case, while the actuator is locked, the reciprocal screws for this limb, which is reciprocal to all the passive joint screws, form a 2-system. One screw, $\hat{\$}_{r1,1}$, can be readily identified as a zero-pitch screw along the line connecting the centres of the two universal joints. The closed form of $\hat{\$}_{r1,1}$ is presented in equation 25. The second reciprocal screw, $\hat{\$}_{r2,1}$, which is also reciprocal to all the passive joint screws can be readily identified as an infinity pitch screw along the normal line of the two planes. The closed form of $\hat{\$}_{r2,1}$ is written as

$$\hat{\$}_{r2,1} = \left[\,0,\ 0,\ 0,\ -\sin(\alpha_1),\ 0,\ -\cos(\alpha_1)\,\right]^T. \quad (38)$$

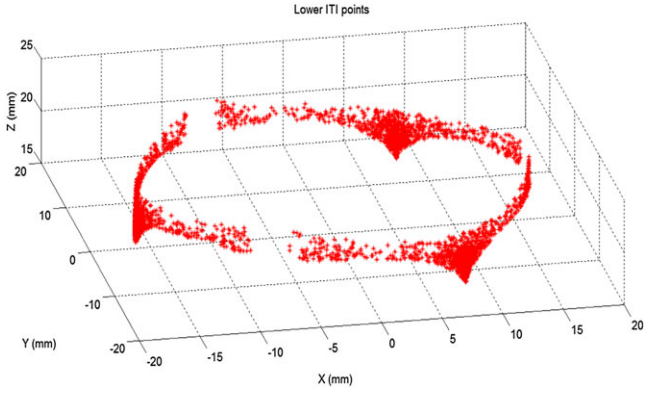

FIGURE 12 Points with input transmission index μ less than 0.2

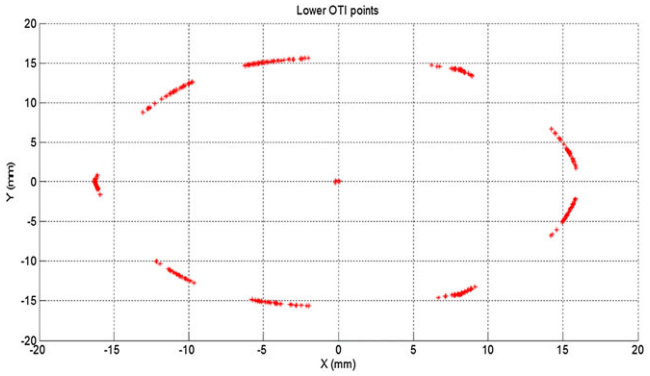

FIGURE 13 Points with output transmission index η less than 0.2

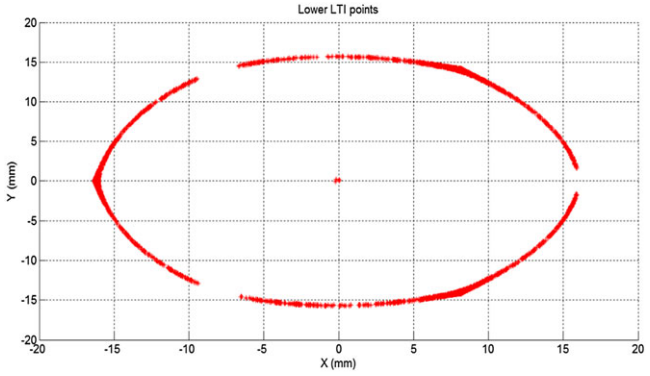

FIGURE 14 Points with local transmission index χ less than 0.2

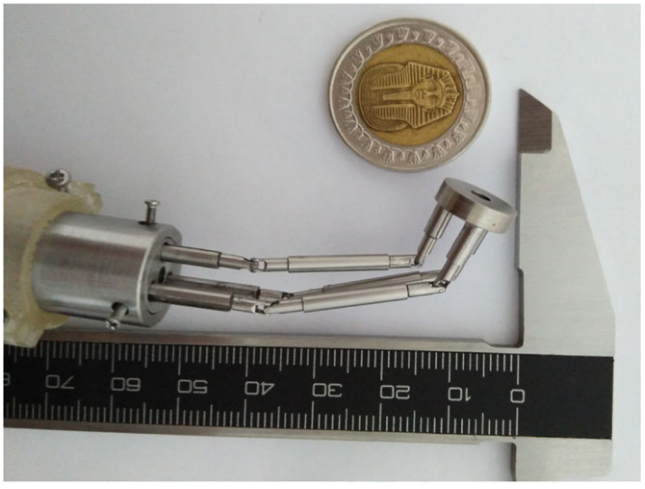

FIGURE 15 Real model of the proposed 3-PUU PM

If the prismatic joint is not locked, the reciprocal screws for this limb form a 1-system, which is a screw that is reciprocal to all the joint screws of the first limb. This reciprocal screw, $\hat{\$}_{rt,1}$, is equal to $\hat{\$}_{r2,1}$ as presented in equation (38).

The second and third limbs have the same structure as the first limb. So, all reciprocal screws $\hat{\$}_{r1,2}$, $\hat{\$}_{r2,2}$, $\hat{\$}_{rt,2}$, $\hat{\$}_{r1,3}$, $\hat{\$}_{r2,3}$ and $\hat{\$}_{rt,3}$ can be identified easily in a closed-form expression in the same manner.

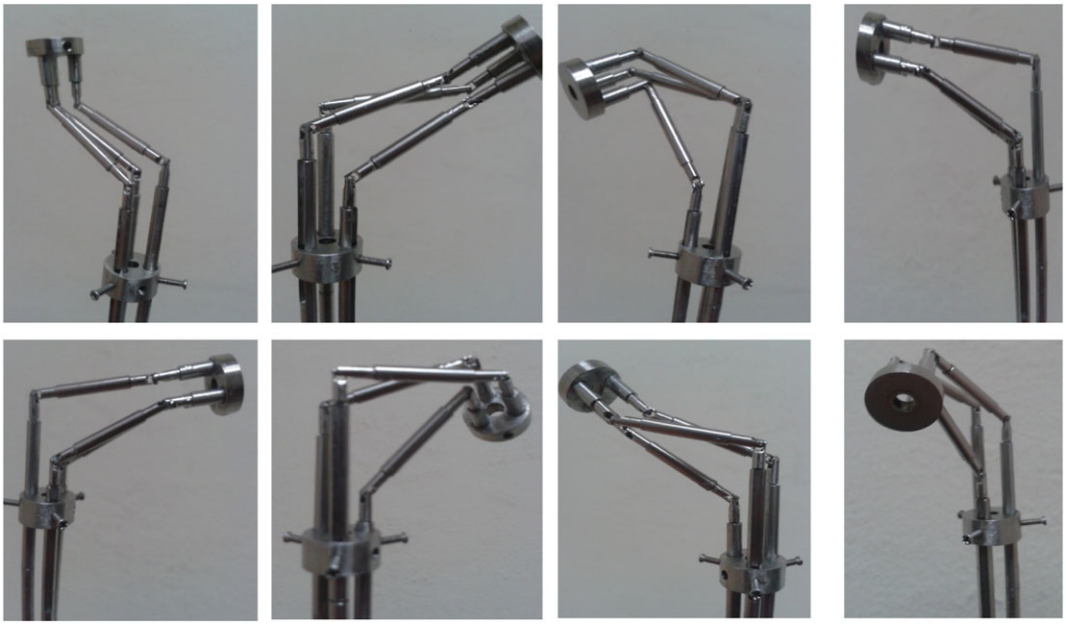

FIGURE 16 Different bending angle configurations of the real 3-PUU PM

FIGURE 17 Experimental system

7 | SINGULAR CONFIGURATIONS OF THE PROPOSED 3-PUU PARALLEL MANIPULATOR

7.1 | Constraint singularities

Constraint singularities arise when the limbs of the (3-PUU) parallel manipulator lose their ability to constrain the movable platform to move with the intended motion.[15] A unit wrench of constraints imposed by the joints of a limb will be represented as a row in the Jacobian of constraint matrix, $\boldsymbol{J}_c$. It can be shown that the Jacobian of constraints $\boldsymbol{J}_c$ is a (3×6) matrix. To properly constrain the moving platform to 3-DOF motion, the rank of $\boldsymbol{J}_c$ should be equal to 3. The Jacobian of constraints $\boldsymbol{J}_c$ of the (3-PUU) parallel surgical manipulator is indicated as

$$\boldsymbol{J}_c = \begin{bmatrix} \hat{\$}^T_{rt,1} \\ \hat{\$}^T_{rt,2} \\ \hat{\$}^T_{rt,3} \end{bmatrix}. \tag{39}$$

Constraint singularities arise when the Jacobian of constraints $\boldsymbol{J}_c$ loses its full rank. These singularities will occur when two or more reciprocal screws from $\hat{\$}^T_{rt,1}$, $\hat{\$}^T_{rt,2}$ and $\hat{\$}^T_{rt,3}$ become linearly dependent. Comparing the analytical expressions for the corresponding components of $\hat{\$}^T_{rt,1}$, $\hat{\$}^T_{rt,2}$ and $\hat{\$}^T_{rt,3}$ reveals that the linear dependence will not occur unless $d_1 = d_2 = d_3$. To validate this result, and considering the mechanical limitations of the joints, a numerical search for points inside the workspace that satisfy the condition for constraint singularities is carried out using MATLAB software. It is found that this condition will

not occur unless $d_1 = d_2 = d_3$. It is found that all the points located on the Z-axis of the fixed reference frame can satisfy this condition. Hence, a constraint singularity configuration occurs when the centre of the movable platform lies on the Z-axis. However, this constraint singularity configuration can be avoided by preventing the equality of d_1, d_2 and d_3 in the control program. In the control program, we added a condition to detect the points of the trajectory at which the equality between input prismatic joints occurs. The program will reject these points and stay at the nearest points at which equality will not occur. Moreover, at the initialization, the control program will make a slight displacement to any prismatic joint. This will produce a minimum bending angle that will not have a significant effect on the insertion process of the proposed 3-PUU parallel manipulator inside the patient's abdomen. Hence, at the initial position, the centre of the movable platform will not be located on the Z-axis, and the constraint singularity is avoided.

7.2 | Architecture singularities

Architecture singularities indicate the conditions for which the actuators cannot control the velocity of the movable platform.[15] The Jacobian of actuations, $\boldsymbol{J_a}$, can be constructed as:

$$\boldsymbol{J_a} = \begin{bmatrix} \hat{\$}^T_{r1,1}/(\hat{\$}^T_{r1,1} \cdot \hat{\$}_{1,1}) \\ \hat{\$}^T_{r1,2}/(\hat{\$}^T_{r1,2} \cdot \hat{\$}_{1,2}) \\ \hat{\$}^T_{r1,3}/(\hat{\$}^T_{r1,3} \cdot \hat{\$}_{1,3}) \end{bmatrix}, \tag{40}$$

where $\boldsymbol{J_a}$ is a (3×6) Jacobian matrix. By complementing the Jacobian of constraints $\boldsymbol{J_c}$ with the Jacobian of actuations $\boldsymbol{J_a}$, the overall (6×6) Jacobian matrix $\boldsymbol{J}$ of the 3-PUU parallel manipulator is obtained. Architecture singularities occur when $\boldsymbol{J}$ loses its full rank but $\boldsymbol{J_c}$ has a full rank of 3. This condition will occur when the linear dependence between the rows of the overall Jacobian $\boldsymbol{J}$ happens. Comparing the analytical expressions for different rows of the overall Jacobian $\boldsymbol{J}$ reveals that no linear dependence occurs and hence no architecture singularity. For further confirmation, a numerical search to find all the architecture singularity configurations is carried out using MATLAB software. It is found that the condition for architecture singularity ($\boldsymbol{J}$ loses its full rank but $\boldsymbol{J_c}$ has a full rank) will not occur inside the workspace of the proposed 3-PUU PM. Hence, the proposed 3-PUU parallel manipulator has no architecture singularity inside its workspace. In the numerical search, the mechanical limitations of the joints are considered.

8 | EVALUATION FOR THE WORKSPACE OF THE PROPOSED 3-PUU PM

The traditional performance indices such as condition number of the Jacobian matrix and manipulability present many inconsistencies for manipulators with mixed rotational and translational DOFs.[16] Therefore, dimensionless and frame-free indices (motion/force transmissibility indices[17,18]) are used to evaluate the performance of the proposed 3-PUU parallel manipulator.

As mentioned above in Section 2, the parallel manipulator 3-PUU consists of three symmetric PUU limbs and the connectivity of each limb is equal to 5. The 5 twists of the joints in each limb are independent. Therefore, these screws have only one reciprocal screw, which is called the constraint wrench. This constraint wrench is provided as $\hat{\$}_{rt,i}$ in equation (36) for $i = 1, 2, 3$. In each limb, only the prismatic joint is actuated. Therefore, the twist of the prismatic joint is called the input twist and is given as $\hat{\$}_{1,i}$ as expressed in equation (21). If the input twist is temporarily locked, a unit wrench is obtained that is called the transmission wrench and is reciprocal to all twists in the limb except the input twist. This transmission wrench, represented by $\hat{\$}_{r1,i}$, is a pure force along the direction of the connecting rod between the two centres of the universal joints and is calculated according to equation (25).

Furthermore, assuming that only 1 prismatic joint is actuated and the other 2 are locked, the 3-PUU PM will have only 1 DOF for the time being. In this case, the unlocked transmission wrench can contribute to the motion of the movable platform. Moreover, the 2 transmission wrenches corresponding to the 2 locked prismatic joints can be regarded as additional constraint wrenches to the movable platform at this time. Accordingly, the output twist of the movable platform $\hat{\$}_{Oi}$,

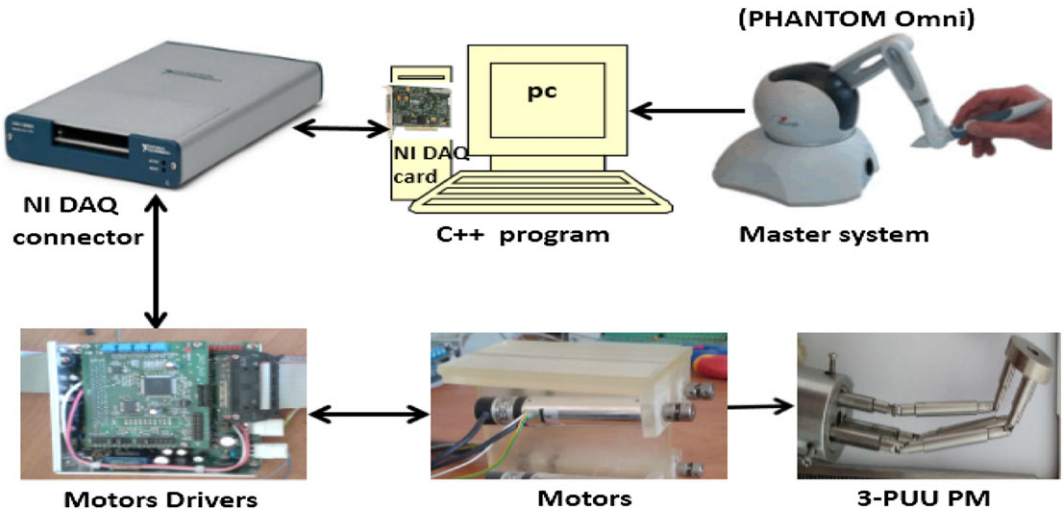

FIGURE 18 Building blocks of the experimental system

related to the unlocked prismatic joint, can be deduced according to the following conditions:

$$\begin{cases} \hat{\$}^T_{r1,j} \cdot \hat{\$}_{Oi} = 0 & \text{for } j = 1,2,3;\ j \neq i. \\ \hat{\$}^T_{rt,k} \cdot \hat{\$}_{Oi} = 0 & \text{for } k = 1,2,3. \end{cases} \tag{41}$$

The screw $\hat{\$}_{Oi}$, which is reciprocal to the 5 independent screws, can be obtained numerically according to the linear algebraic procedure presented by Dai and Jones.[19] To summarize, the 3-PUU parallel manipulator has 3 input twists $\hat{\$}_{1,i}$, 3 corresponding transmission wrenches $\hat{\$}_{r1,i}$, 3 constraint wrenches $\hat{\$}_{rt,i}$ and 3 output twists $\hat{\$}_{Oi}$. All these twists and wrenches will be used in calculating the motion/force transmissibility indices. There are 3 kinds of motion/force transmissibility indices.[17,18] These kinds are input, output and local transmission index.

The values of the transmissibility indices range from 0 to 1. A large value of the index indicates better performance in transmission and vice versa. The points near a singularity will have an index with a low value near zero. Considering the mechanical limitations of the joints, a numerical search inside the workspace for points with a low index value is carried out using a MATLAB program. Figure 12 illustrates the points with input transmission index less than 0.2. Also, Figure 13 shows the points with output transmission index less than 0.2. Moreover, Figure 14 illustrates the points with local transmission index less than 0.2. These 3 figures show that all workspace points with low transmissibility indices are located near the boundary of the workspace of the proposed manipulator. Therefore, the proposed 3-PUU PM has workspace points with perfect input, output and local transmission.

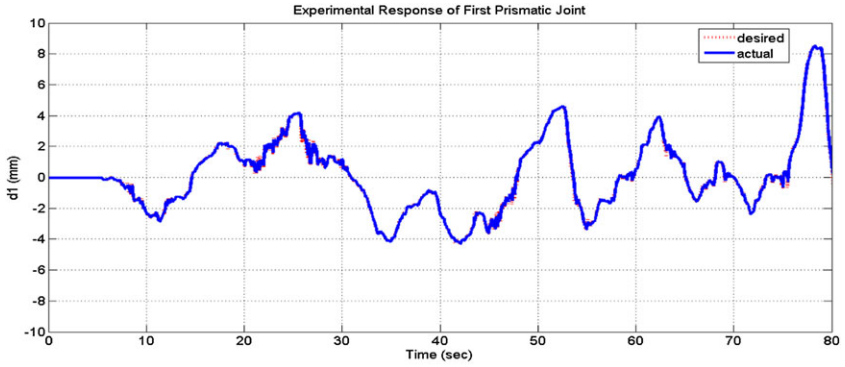

(A)

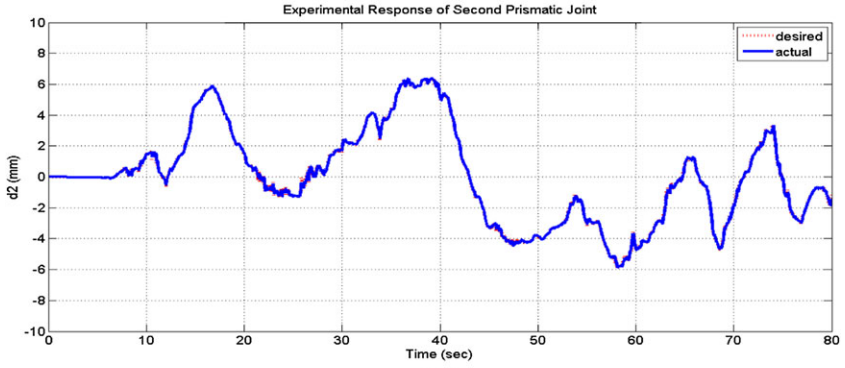

(B)

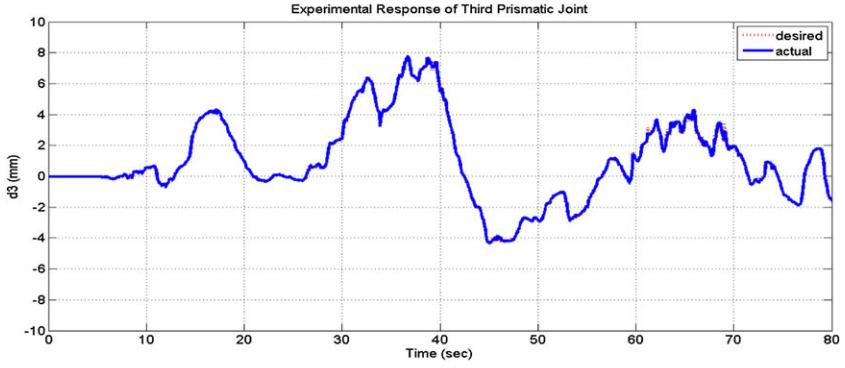

(C)

FIGURE 19 Experimental response of the actuators: (a) d_1 response, (b) d_2 response and (c) d_3 response

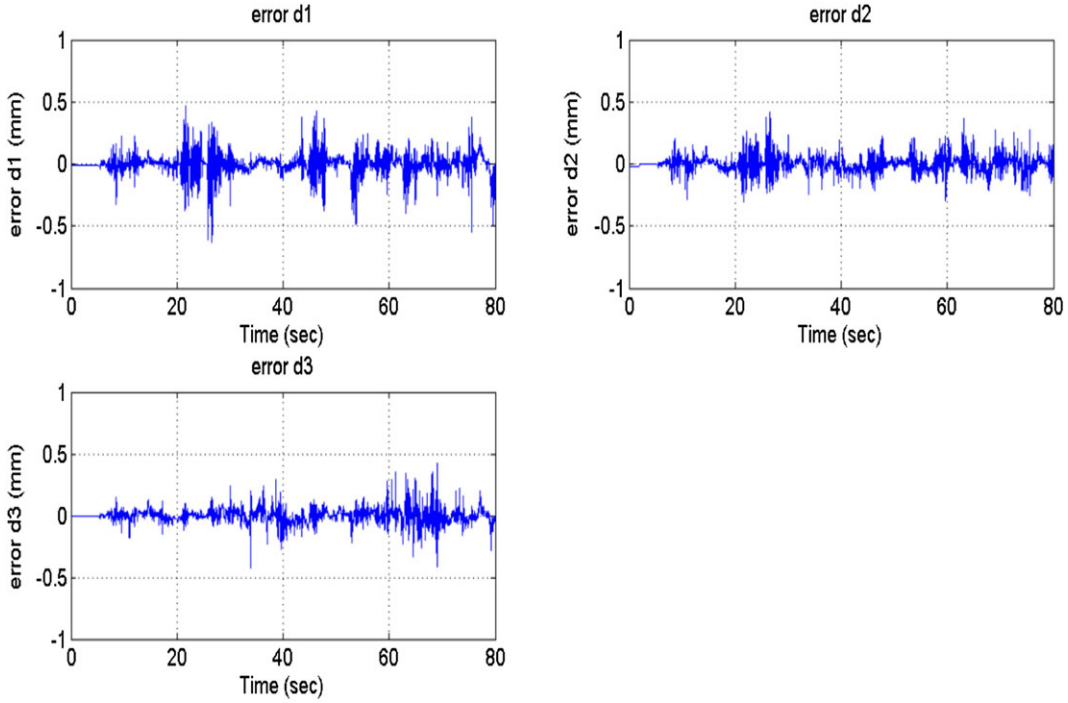

FIGURE 20 Error between the desired and actual values of the actuators

9 | EXPERIMENTAL SETUP AND SYSTEM VERIFICATION

In order to validate the proposed manipulator and its bending capability, a real model of the proposed manipulator is manufactured from annealed stainless steel as shown in Figure 15. The real validation is presented in Figure 16, which indicates the ability of the proposed manipulator (3-PUU) to bend in any direction with a large bending angle that can exceed ±90°.

In order to investigate the feasibility of the teleoperation system that uses the manufactured 3-DOF parallel manipulator (3-PUU) as a slave robot, a practical experiment has been performed using a scaling technique and PID controller. An experimental setup is established as illustrated in Figure 17. Moreover, Figure 18 presents the block diagram of the system and illustrates how the components of the system are arranged. Also, it provides the signal flow between the system's elements.

An experiment has been accomplished as shown in the video at the link: https://www.dropbox.com/s/ng9aneo1klr7n6m/Media_3PUU.mp4?dl=0. This video shows a practical implementation of the whole teleoperated system in which the PHANTOM-Omni haptic device is used as the master robot and the proposed 3-PUU parallel manipulator as the slave one. A C++ program is developed for commanding the three prismatic joints according to the motion of the master device. A PID controller is used to control the system's position. For easy and comfortable operation, the operator can select the current position as the zero position. So, by using a push button (home position button), the operator can determine the starting point, and the program takes this point as the origin point for the operation. Before pressing the push button, any movement of the master device will not be mapped to the slave side. An experiment with the proposed surgical manipulator has been performed. The operator presses the push button after 5.4 seconds, so there is no movement of the actuators before that time. After pressing the push button (home position button), the movement of the master device is mapped to the slave side using the scaling technique. [20]

Figure 19 illustrates the experimental response of the 3 actuators as a result of moving the master device. The desired values are obtained from the inverse kinematics solution, and the actual values are measured using the incremental encoder of each active prismatic joint. This figure illustrates the feasibility of the new 3-DOF parallel manipulator (3-PUU). Moreover, it proves that the control algorithm can achieve a trajectory tracking.

Figure 20 presents the tracking error between the desired and actual values of the actuators' positions. It can be noticed that the maximum error in each actuated prismatic joint is less than 0.6 mm.

10 | CONCLUSIONS

The article proposes a new 3-DOF (2 rotational and 1 translational DOF) endoscopic parallel manipulator. It consists of three limbs having a unique arrangement of joints connecting the fixed platform with the movable one. This unique arrangement enables unprecedentedly large bending angles, ±90° in all directions, and a workspace almost free from interior singularities. The virtual prototype is constructed using ADAMS software. The results indicate the ability of the proposed manipulator (3-PUU) to bend in any direction with a large bending angle that can exceed ±90°. A closed-form solution for the inverse kinematics is obtained analytically. Moreover, the forward kinematics solution

is obtained numerically. The singularity analysis of the new parallel manipulator is investigated using a geometrical/analytical approach for reciprocal screws. Moreover, evaluation of the workspace is achieved using motion/force transmissibility indices. The results show that all workspace points with low transmissibility indices are located near the boundary of the workspace. Therefore, the proposed 3-PUU PM has workspace points with perfect motion/force transmission. The complete experimental setup of the teleoperated surgical system has been built using the 3-PUU parallel manipulator as the slave robot and a PHANTOM-Omni haptic device as the master robot. In this initial stage, a PID controller is utilized to control the motion of the slave robot. The experimental results obtained confirmed the feasibility of the surgical manipulator that has bending angles of more than ±90° in all directions. Finally, the results ensure the efficiency of the designed controller in spanning the slave workspace with good tracking. As a future work, a hybrid intelligent control system will be used to improve the performance. Also, a gripper with force sensor will be attached to the surgical manipulator.

ORCID

Alaa Khalifa http://orcid.org/0000-0002-1617-5409

REFERENCES

1. Guthart G, Salisbury Jr JK. The intuitivetm telesurgery system: Overview and application. In: IEEE International Conference on Robotics and Automation (ICRA); 2000; San Francisco, CA:618-621.
2. Berkelman P, Ma J. A compact modular teleoperated robot system for laparoscopic surgery. *The Int J Rob Res*. 2009;28(9):1198-1215.
3. Arata J, Mitsuishi M, Warisawa S, Tanaka K, Yoshizawa T, Hashizume M. Development of a dexterous minimally-invasive surgical system with augmented force feedback capability. In: 2005 IEEE/RSJ International Conference on Intelligent Robots and Systems. IROS 2005 IEEE; 2005; Alberta, Canada:3207-3212.
4. Ishii C, Kobayashi K, Kamei Y, Nishitani Y. Robotic forceps manipulator with a novel bending mechanism. *IEEE/ASME Trans Mechatron*. 2010;15(5):671-684.
5. Yamashita H, Iimura A, Aoki E, Suzuki T, Nakazawa T, Kobayashi E, Hashizume M, Sakuma I, Dohi T. Development of endoscopic forceps manipulator using multi-slider linkage mechanisms. *Journal of Japan Society of Computer Aided Surgery*. 2005;7(2):201-204.
6. Röse A, Wohlleber C, Kassner S, Schlaak HF, Werthschützky R. A novel piezoelectric driven laparoscopic instrument with multiple degree of freedom parallel kinematic structure. In: 2009 IEEE/RSJ International Conference on Intelligent Robots and Systems. IROS 2009. IEEE; 2009; St. Louis, MO:2162-2167.
7. Ibrahim K, Ramadan A, Fanni M, Kobayashi Y, Abo-Ismail A, Fujie MG. Screw theory based-design and tracking control of an endoscopic parallel manipulator for laparoscopic surgery. In: 2013 IEEE International Conference on Robotics and Automation (ICRA). IEEE; 2013; Karlsruhe, Germany:2491-2496.
8. Ibrahim K, Ramadan A, Fanni M, Kobayashi Y, Abo-Ismail A, Fujie MG. Development of a new 4-DOF endoscopic parallel manipulator based on screw theory for laparoscopic surgery. *Mechatronics*. 2015;28:4-17.
9. Khalifa A, Fanni M, Mohamed AM. Geometrical/analytical approach for reciprocal screw-based singularity analysis of a novel dexterous minimally invasive manipulator. *Rob Auton Syst*. 2017;98:56-66.
10. Li Y, Xu Q. Kinematics and inverse dynamics analysis for a general 3-PRS spatial parallel mechanism. *Robotica*. 2005;23(02):219-229.
11. Tsai L-W, Joshi S. Kinematic analysis of 3-DOF position mechanisms for use in hybrid kinematic machines. *J Mech Des*. 2002;124(2):245-253.
12. Liping W, Huayang X, Liwen G, Yu Z. A novel 3-PUU parallel mechanism and its kinematic issues. *Rob Comput-Integr Manuf*. 2016;42:86-102.
13. Tsai L-W. *Robot Analysis: The Mechanics of Serial and Parallel Manipulators*. New York: John Wiley & Sons; 1999.
14. MIYOSHI KIKAI CO. LTD. Available from: http://www.miyoshikikai.co.jp/en/." Last accessed Dec. 17, 2017.
15. Joshi SA, Tsai L-W. Jacobian analysis of limited-DOF parallel manipulators. *J Mech Des*. 2002;124(2):254-258.
16. Merlet J-P. Jacobian, manipulability, condition number, and accuracy of parallel robots. *J Mech Des*. 2006;128(1):199-206.
17. Wang J, Wu C, Liu X-J. Performance evaluation of parallel manipulators: Motion/force transmissibility and its index. *Mech Mach Theory*. 2010;45(10):1462-1476.
18. Wu C, Liu X-J, Wang L, Wang J. Optimal design of spherical 5R parallel manipulators considering the motion/force transmissibility. *J Mech Des*. 2010;132(3):031002-1:10.
19. Dai JS, Jones JR. A linear algebraic procedure in obtaining reciprocal screw systems. *J Field Rob*. 2003;20(7):401-412.
20. Mamdouh M, Ramadan AA. Development of a teleoperation system with a new workspace spanning technique. In: 2012 IEEE International Conference on Robotics and Biomimetics (ROBIO) IEEE; 2012; Guangzhou, China:1570-1575.

How to cite this article: Khalifa A, Fanni M, Mohamed AM, Miyashita T. Development of a new 3-DOF parallel manipulator for minimally invasive surgery. *Int J Med Robotics Comput Assist Surg*. 2018;14:e1901. https://doi.org/10.1002/rcs.1901